GATA1 knockout in human pluripotent stem cells generates enhanced neutrophils to investigate extracellular trap formation

Thomas C. Harper[1*], Elaine M. Oberlick[2], Tomas J. Smith[2], Duncan E. Nunes[2], Mark A. Bray[1], Seonmi Park[1], Corey D. Driscoll[2], Sarah F. Mowbray[2], Christophe Antczak[1]

[1]Chemical Biology and Therapeutics, Novartis Institutes for BioMedical Research, Cambridge, MA. United States

[2]Respiratory Disease Area, Novartis Institutes for BioMedical Research, Cambridge, MA. United States

*tomdomma@gmail.com

Abstract

Human pluripotent stem cell (hPSC)-derived tissues can be used to model diseases and validate targets in cell types that are challenging to harvest and study at-scale, such as neutrophils. Neutrophil dysregulation, specifically unbalanced neutrophil extracellular trap (NET) formation, plays a critical role in the prognosis and progression of multiple diseases, including COVID-19. hPSCs can provide a limitless supply of neutrophils (iNeutrophils) to study these processes and discover and validate targets *in vitro*. However, current iNeutrophil differentiation protocols are inefficient and generate heterogeneous cultures consisting of different granulocytes and precursors, which can confound the study of neutrophil biology. Here, we describe a method to dramatically improve iNeutrophils' yield, purity, functionality, and maturity through the deletion of the transcription factor *GATA1*. *GATA1* knockout (KO) iNeutrophils are nearly identical to primary neutrophils in cell surface marker expression, morphology, and host defense functions. Unlike wild type (WT) iNeutrophils, *GATA1* KO iNeutrophils generate NETs in response to the physiologic stimulant lipid polysaccharide (LPS), suggesting they could be used as a more accurate model when performing small-molecule screens to find NET inhibitors. Furthermore, we demonstrate that *GATA1* KO iNeutrophils are a powerful tool in quickly and definitively determining involvement of a given protein in NET formation.

Introduction

Neutrophils are the most abundant immune cells in the human body and make up approximately 70% of circulating leukocytes. They migrate to the site of infections where they recruit other immune cells, and independently destroy invading microorganisms through phagocytosis, the release of granules, and the formation of neutrophil extracellular traps (NETs) (1,2).

While neutrophils are an important first line of defense in the innate immune system, their overactivation can have a proportionally negative impact on many diseases and affect numerous organ systems. The dysregulation of neutrophils is correlated with the progression of multiple diseases including rheumatoid arthritis, atherosclerosis, psoriasis, chronic obstructive pulmonary disease, and gallstone formation (3–7).

COVID-19 clearly establishes the link between overactive neutrophils and disease severity and highlights the need for improved methods to model neutrophil dysregulation. SARS-CoV-2, the virus which causes COVID-19, has been shown to directly induce NETs (8,9) and the overproduction of NETs and neutrophil reactive oxygen species (ROS) exacerbate COVID-19 complications including blood clots, cytokine storm, organ damage, and respiratory failure (10–13). Unsurprisingly, there is a strong positive correlation between NET production, disease severity and patient outcome (14,15).

While inhibiting overactive neutrophils has the potential to mitigate COVID-19 severity (15–17), the nature of primary neutrophils severely restricts their utility in drug discovery. Primary neutrophils, like all donor tissues, are limited by access and cross-patient variability, and pose the challenges of not proliferating or cryopreserving and survive *ex vivo* for less than 24 hours (18). These shortcomings preclude large-scale drug screening and make unbiased genetic screens and target validation experiments using CRISPR/Cas9 impossible.

Human pluripotent stem cells (hPSCs) provide an inexhaustible source of material that can overcome these challenges. hPSCs self-renew indefinitely, can be differentiated into a variety of highly relevant cell types, and are easy to genetically modify. hPSC-derived cells have been successfully used in a variety of pharmaceutical efforts, ranging from high-throughput phenotypic drug screens to model and correct neurological disorders, to the generation of hepatocytes to screen drug-mediated toxicity (19,20). The production of homogeneous cultures of mature cells is crucial for assay relevance and reproducibility. Unfortunately, current protocols to produce hPSC-derived neutrophils (iNeutrophils) generate a heterogeneous combination of hematopoietic progenitors and cells resembling neutrophils, eosinophils, and basophils (21–25).

Based on transcriptional analysis of sorted iNeutrophils along with mouse genetic studies, we surmised that the deletion of *GATA1*, a transcription factor important for the development of eosinophils and basophils, would force hPSC-derived granulocytes into a neutrophil specific program and eliminate contaminating cells (26,27). We demonstrate that knocking out *GATA1* in H1 human embryonic stem cells (hESCs) using CRISPR/Cas9 (*GATA1* KO) followed by granulocyte differentiation produces pure populations of iNeutrophils that are nearly identical to their primary counterparts. Compared to wild type (WT) iNeutrophils, *GATA1* KO iNeutrophils have dramatically improved levels of the neutrophil surface markers CD182, CD66b, CD15, CD16 and CD11b and retain their host defense functions including phagocytosis, ROS production and myeloperoxidase (MPO) activity. Unlike WT iNeutrophils, *GATA1* KO iNeutrophils form NETs after treatment with the physiologic NET stimulant lipid polysaccharide (LPS). Furthermore, *GATA1* KO iNeutrophils can be further genetically manipulated through CRISPR/Cas9 to evaluate the role of individual genes in neutrophil functions. *GATA1* KO iNeutrophils with deletion of *CYBB*, which encodes a protein involved in NET formation, exhibit reduced NET formation in response to NET stimulants.

Materials and Methods

Neutrophil differentiation

Differentiation was adapted from previously published protocols (28,29). All cells were cultured in humidified tissue culture incubators at 37°C with 5% $C0_2$. H1 hESCs were maintained on Matrigel (Corning, 354277) coated dishes using mTeSR Plus media (StemCell Tech, 100-0276). The day before induction (Day -1), cells were dissociated into 100 to 300 µm clumps using ReLeSR (StemCell Tech, 05872) and plated onto hematopoietic Matrigel (Corning, 354234) coated 6 cm dishes in mTeSR Plus media with 10 µM Y-27632 (Tocris, 1254). On Day 0, mTeSR Plus was removed and cells were induced with Base Media 1 (StemPro 34 SFM Media (Gibco, 10639011) containing 1x GlutaMAX (Gibco, 35050079), 0.45 mM aMTG (Sigma-Aldrich, M6145), 200 µg/ml Transferrin (Sigma-Aldrich, 10652202001), and 88 µg/ml L-Ascorbic Acid (Sigma-Aldrich, A4403)) supplemented with 5 ng/ml BMP4 (R&D Systems, 314-BP), 50 ng/ml VEGF (R&D Systems, 293-VE) and 2 µM CHIR99021 (Tocris, 4423). Cells were incubated for two days. On Day 2, cells were refreshed with Base Media 1 plus 5 ng/ml BMP4, 50 ng/ml VEGF, and 20 ng/ml bFGF (R&D Systems, 233-FB). On Day 4, cells were again refreshed with Base Media 1 plus 15 ng/ml VEGF and 5 ng/ml bFGF. On Day 6, media was replaced with Base Media 2 (StemPro 34 SFM Media containing 1x GlutaMAX, 0.4 mM aMTG, 150 µg/ml Transferrin, and 50 µg/ml L-Ascorbic Acid)) supplemented with Growth Factor Cocktail (5 ng/ml BMP4, 5 ng/ml bFGF, 10 ng/ml IL-6 (R&D systems, 206-IL), 10 ng/ml Flt3L (PeproTech, 300-19), 5 ng/ml IL-11 (PeproTech, 200-11), 25 ng/ml IGF-1 (R&D Systems, 291-G1), 30 ng/ml IL-3 (R&D Systems, 203-IL), 30 ng/ml TPO (PeproTech, 300-18), 50 ng/ml VEGF, 100 ng/ml SCF (R&D Systems, 255-SC), 20 ng/ml SHH (PeproTech, 100-45) and 10 µg/ml Angiotensin II (Sigma-Aldrich, A9525)). After one or two days, cells began to shed away from the adherent monolayer, so during each media change, used media containing floating cells was collected, centrifuged at 300 x g for 10 minutes to pellet cells, resuspended in fresh media, and returned to their original dishes. Media was changed every other day using Base Media 2 plus Growth Factor Cocktail until Day 12, when floating cells were collected and plated into new 6 cm dishes with Maturation Media (RPMI (Gibco, 61870036), 10% FBS, 1 mM Sodium Pyruvate (Gibco, 11360070), 55 µM b-Mercapto, 25 mM HEPES (Gibco, 15630130), and 100 ng/ml G-CSF (Peprotech, 300-23)). Maturation Media was changed every other day until Day 18 when G-CSF was removed for 24 hours before experiments on day 19 to avoid G-CSF related stimulation. At harvest, cells were strained through a 15 µm filter (pluriSelect, 43-50015-03) to remove debris followed by centrifugation for 10 minutes at 300 x g to pellet cells. Cell numbers were quantified using a Beckman Coulter Vi-Cell XR cell viability analyzer.

***GATA1* KO using CRISPR/Cas9**

An Amaxa Nucleofector II Device and Nucleofector Kit (Lonza, VPH-5012) were used to transiently express 5 µg of *GATA1* gRNA plasmid (gRNA sequence: ggtgtggaggacaccagagcagg) containing a puromycin resistance gene into 1 x 10^6 H1 hESCs constitutively expressing *Cas9* from the *AAVS1* locus. After nucleofection, cells were plated onto a 6 cm dish in mTeSR plus media with 10 µM Y-27632, and

two days later selected using 1 µg/ml puromycin for 2 days, clonally expanded, genomic DNA extracted (Invitrogen, K1820-1), and target locus PCR amplified (forward primer: gatgcaggagggaaaagagagga, reverse primer: gcaaccaccacatacttccagt) using Platinum *Taq* DNA Polymerase (Invitrogen, 11304011). Amplicons were analyzed using Sanger sequencing and clones with frame shift deletions picked for expansion. All experiments were performed with a *GATA1* KO clone containing a 13 base-pair frame shift deletion (Figure S1). *GATA1* is located on the X-chromosome so only one allele of H1 hESCs (XY karyotype) required editing.

Hematoxylin and eosin staining

To visualize morphology, 1.5 x 10^5 cells were suspended in 200 ul PBS plus 1% BSA (Sigma-Aldrich, A9576) and spun onto glass slides using a Thermo Scientific Cytospin 4 centrifuge at 300 x g for 5 minutes, processed through a Siemens Hematek 2000 for staining and sealed / preserved using DPX mounting media (Sigma-Aldrich, 06522). Stained cells were then visualized using a Nikon Eclipse Ci-L microscope.

Flow cytometry

5 x 10^5 cells per condition were distributed into a 96-well v-bottom plate (Corning, 3357), washed with stain buffer (BD Biosciences, 554657), then incubated with 200 µl fluorophore-conjugated antibodies diluted in stain buffer for 30 minutes on ice. Cells were then washed two times and fixed with 4% paraformaldehyde (Electron Microscopy Services, 15710) diluted in PBS for 30 minutes followed by two more washes. For washes, 200 µl of stain buffer were added to each sample well followed by centrifugation at 300 x g for 5 minutes at 4°C. All steps were performed in dark conditions and on ice. Antigen specific antibodies reacted to UltraComp eBeads (Invitrogen, 01-3333-42) were used as single-color compensation controls and corresponding isotype controls were included for each antigen specific antibody. Experiment was run using a Yeti (Propel Labs) flow cytometer and analysis was performed using FlowJo software. To calculate positive marker expression, a cut off of no more than 3% isotype background was used. A list of antibodies used is available in Tables S1A and S1B.

RT-qPCR

Cells were harvested on Days 0, 6 and 12 of the differentiation and RNA extracted and purified using the RNeasy Mini Kit (Qiagen, 74104), reverse transcribed using SuperScript IV Reverse Transcriptase (Invitrogen, 18090010), and gene expression analyzed by TaqMan assay using Fast Advanced Master Mix (Applied Biosystems, 4444963) and the QuantStudio Flex Real-Time PCR System (Applied Biosystems, 4485701). Fold-changes relative to WT H1 hESCs were calculated using the delta-delta Ct method and normalized using the housekeeping gene *GAPDH*. For each time-point, the experiment was performed on three independent differentiations using technical triplicates. A list of TaqMan probes used is available in Supplemental Table 2.

ROS production

ROS release was measured using the CM-H2DCFDA (General Oxidative Stress Indicator) kit (Invitrogen, C6827) following the manufacturer's protocol. Briefly, cells were resuspended to $1x10^6$ cells/ml in warm Hanks Balanced Salt Solution (HBSS, Gibco, 14025-092) with 5 µM CM-H2DCFDA dye, incubated at 37°C for 20 minutes, then washed with HBSS. Sotrastaurin was transferred to black-walled, clear-bottomed 384-well cell plates (Greiner, 781091) using the LabCyte Echo for a final concentration of 30 µM, then $2.5 x10^4$ cells / well were added directly into plates and pre-treated for 30 minutes at 37°C. Plates were washed with HBSS, then treated with 10 nM PMA stimulant or DMSO for one hour at 37°C. Fluorescence of 2',7'-dichlorofluorescein generated by ROS-induced oxidation of the DCFDA reagent to was measured on a CLARIOstar plate reader at 488-14 / 535-30 excitation / emission, then adjusted down by 75% of highest well to bring all wells into range. Mean fluorescence from cell-free wells was subtracted to control for background fluorescence. Experiment was performed on four independent differentiations and three independent donors in at least five technical replicates per experiment.

Primary neutrophil isolation

Peripheral blood from healthy donors (defined as not having asthma or allergies and not having taken NSAIDS within the previous 5 days) was obtained at Novartis Institutes of Biomedical Research using informed consent under an approved Institutional Review Board research protocol. Fresh blood was EDTA anti-coagulated and used within two hours of donation. Primary donor neutrophils were extracted using Ficoll-density centrifugation. Per 10 ml of fresh blood, 5 ml of PBS and 5 ml of 4% Dextran (Sigma-Aldrich, 31392-50G) in PBS (Gibco, 10010-023) were added and mixed in a 50 ml tube by gently by inverting 2.5 times, then allowed to settle for 30 minutes at room temperature, separating into a dense layer topped with a supernatant containing leukocytes. 75% of the supernatant volume of Ficoll-Paque Premium (Sigma-Aldrich, GE17-5442-03) was added to a new 50 ml falcon tube. The supernatant was carefully transferred on top of the Ficoll, then centrifuged at 650 x g for 20 minutes at room temperature, with a low acceleration (2) and no brake (deceleration set to 0). The supernatant was removed, then the pellet was resuspended in 10 ml of water (Ultrapure diH2O) and mixed no more than 30 seconds to lyse red blood cells. Then 10 ml of 2 x PBS (made from 10 x PBS Gibco, 70011044) was added, and tubes were centrifuged 300 x g for 10 minutes at room temperature (reset acceleration and deceleration to 9). The supernatant was aspirated, and the pellet containing granulocytes was resuspended in IMDM (Gibco, 21056023) and counted with a ViCell Cell Counter. For the ROS assay, primary neutrophils were resuspended in Hanks Balanced Salt Solution (HBSS, Gibco, 14025-092) and counted.

Phagocytosis

Primary neutrophils or iNeutrophils were seeded in V-bottom 96-well plates (Greiner, 651201) at $5 x 10^5$ cells / well in 100 µl of IMDM (Gibco, 21056023), then treated with either DMSO or 20 µM cytochalasin D (Sigma-Aldrick, C8273) and incubated at 37°C for 1 hour. During the incubation, 500 µl of Fluoresbrite YG Carboxylate Microspheres 1.75 µm (PolySciences, 17687-5) were opsonized in 4500 µl of Normal Human Serum (GeminiBio, 100-110) diluted 50 / 50 in PBS. Fluorescent particles were incubated at

room temperature in the dark for 5 minutes then spun down at 300 x g. The supernatant was removed and the opsonization process was repeated one more time. After the second spin the beads were resuspended in 5 ml of 50 / 50 normal human serum / PBS mixture and 100 µl of the opsonized beads were added per well and incubated for 30 minutes at 37°C. After incubation, the cells were spun down at 300 x g in a 4°C centrifuge and the supernatant was removed. Cells were fixed for 5 minutes with 100 µl / well 4% paraformaldehyde in PBS, then washed twice with ice-cold PBS. After the second wash the supernatant was removed and 200 µl of PBS, followed by 100 µl of 0.4% trypan blue, was added to each well. Cells were then analyzed by flow cytometry for uptake of fluorescent particles. Experiment was performed on at least three independent differentiations and three independent donors in at least technical triplicates.

MPO activity

The MPO activity of cell lysates was measured using an EnzChek Myeloperoxidase Activity Assay Kit (Invitrogen, E33856) following manufacturer's instructions. Briefly, cells were resuspended in at 5 x 10^5 cells / ml in PBS and lysed through freeze thaw cycles and 25 ul added to each well of a 384-well dish (PerkinElmer, 6007270). Chlorination was measured by addition of AFP reagent and fluorescence was measured using a BMG PHERAstar at excitation and emission wavelengths of 485 nm and 520 nm, respectively. Mean fluorescence from cell-free wells was subtracted from experiment wells to control for background fluorescence. Experiments were performed on three independent differentiations and three independent donors using at least technical triplicates.

NET formation

iNeutrophils or primary neutrophils were plated in IMDM (Gibco, 21056023) at a density of 5 x 10^4 cells per well in ultra-low base 384-well dishes (Aurora, ABD241001A) and pre-treated with DMSO, 20 µg/ml GSK484 (BioVision, B1035), 20 µg/ml sotrastaurin (Selleck Chemicals, S2791), 20 µg/ml diphenyleneiodonium chloride (DPI, Sigma-Aldrich, D2926), 100 µg/ml 4-aminobenzoic acid hydrazide (4-ABAH, Sigma-Aldrich, A41909) or 20 µg/ml disulfiram (Tocris, 3807) for 1 hour followed by 3 hours of stimulation using 50 nM phorbol myristate acetate (PMA, Sigma-Aldrich, P1585), 25 µg/ml Lipopolysaccharide (LPS) O128:B12 , (Sigma-Aldrich, L2887) or 5 µg/ml A23187 (Sigma-Aldrich, C7522) at 37°C. A fix/perm/stain solution was then added for a final concentration of 2% paraformaldehyde (Electron Microscopy Services, 15710), 0.1% Triton X100 (Sigma-Aldrich, X100-100ML) and 50 nM Sytox Green (Invitrogen, S7020). Nine fields per well were imaged using the Yokogawa CV8000 automated microscope. Image features were extracted using CellProfiler (version 4.2.4) followed by analysis using custom supervised machine learning software to classify NET versus non-NET nuclei based on nuclei features including size, shape, intensity, etc. Experiments were performed on at least three independent differentiations and three independent donors in at least technical triplicates.

Results

Conventional cytokine differentiation yields heterogeneous iNeutrophils

First, we generated hemogenic endothelium using cytokines and small molecules following previously published protocols (28,29) (Figures 1A and 1B). Next, we supplemented the hematopoietic progenitor's media with G-CSF to push the cells towards the neutrophil lineage (30). Hematoxylin and eosin images of Day 19 iNeutrophils revealed a variety of cell types with morphologies consistent with different granulocytes and progenitors (Figure 1C). Flow cytometry analysis identified two major populations distinguishable by size (forward-scatter) and granularity (side-scatter) (Figure 1D). The larger, more granular cells expressed high levels of the non-neutrophil granulocyte surface markers Siglec-8 and CD193, while the smaller, less granular cells expressed high levels of the neutrophil surface markers CD15 and CD16. These smaller, less granular cells also expressed lower levels of the hematopoietic progenitor marker CD33 and higher levels of the mature granulocyte marker CD66b, suggesting this population is immunophenotypically like mature neutrophils. As expected, the pan-hematopoietic marker CD45 was similar in both populations of floating cells (Figures 1E and 1F).

Next, we sorted the low and high forward- and side-scatter populations using FACS and compared the transcript levels of five regulators of granulocyte specification. While most regulators had a five-fold difference or less in transcript levels between the two groups, *GATA1* was upregulated more than 25-fold in the non-neutrophil population (Figure 1G). Studies in mice demonstrate that *Gata1* is critical in the development of eosinophils and basophils, and while it is expressed in the common myeloid progenitor, it is dispensable for the differentiation and function of neutrophils (26,27). These findings suggest that *GATA1* is a key gene responsible for specifying the non-neutrophil population and downregulation could restrict cells toward the desired neutrophil fate.

GATA1 KO improves iNeutrophil specification

We devised a novel differentiation approach by deleting *GATA1* in our hESCs to restrict their differentiation capacity to the desired neutrophil cell type. Like their WT counterparts, *GATA1* KO hESCs were able to self-renew and expressed high levels of the pluripotency markers *OCT4* and *NANOG* (Figure 2A). Upon differentiation, both the WT and *GATA1* KO cells downregulated these pluripotency genes and began expressing the hematopoietic transcription regulators *SPI1* and *GFI1* (Figure 2B). By Day 12, the WT and *GATA1* KO hematopoietic progenitors showed differences in gene expression suggesting the *GATA1* KO cells were more neutrophil-like than the WT cells. The Day 12 *GATA1* KO hematopoietic progenitors expressed higher levels of the neutrophil genes *AZU1*, *AQP9*, *ELANE* and *MPO*, and expressed lower levels of the eosinophil and basophil-specific gene *CLC* (Figures 2C and 2D). Like primary neutrophils, Day 19 WT and *GATA1* KO iNeutrophils expressed low levels of mRNA which prevented us from comparing gene expression.

Hematoxylin and eosin images of Day 19 *GATA1* KO iNeutrophils showed a dramatic increase in the number of cells with the classic neutrophil multilobulated nuclear morphology (Figures 2E and S2). Furthermore, the *GATA1* KO cells generated on average 17 x 10^6 cells from each 6 cm dish, more than

double that of the WT cells, demonstrating that this improved differentiation method can produce at-scale numbers of homogeneous iNeutrophils.

GATA1 KO iNeutrophils share many characteristics of primary neutrophils

Surface proteins on immune cells mediate cell communication and signal transduction and are often used to distinguish different granulocytes. We used fluorophore-conjugated antibodies specific to basophil, eosinophil, and neutrophil surface proteins (Figure 3A) and flow cytometry to compare WT and *GATA1* KO iNeutrophils versus primary neutrophils. Staining WT iNeutrophils using antibodies against Siglec-8 showed that roughly 50% of the cells adopted an eosinophil phenotype, supported further by the co-expression of CD193 in 25% of the total floating cells (Figures 3B and S3A). Additionally, 26% of the WT cells expressed the non-neutrophil granulocyte marker CD49d. Alternatively, 5% of the *GATA1* KO iNeutrophils expressed Siglec-8 and 4% co-expressed CD193. Only 6% of the *GATA1* KO iNeutrophils expressed CD49d (Figures 3B and S3A).

While more than 80% of the WT iNeutrophils are CD182 and CD11b positive, fewer expressed the mature neutrophil markers CD15 (50%) and CD16 (29%), and only 22% express the mature granulocyte marker CD66b (Figure 3C).

Alternatively, we saw a dramatic increase in not only the number of CD182 (94%) and CD11b (98%) positive *GATA1* KO iNeutrophils, but also in the magnitude of signal (Figure 3C). More than 90% of the *GATA1* KO iNeutrophils expressed CD15 and CD16, and more than 85% expressed CD66b. Multiplexed staining revealed that more than 80% of the *GATA1* KO iNeutrophils were co-positive for the neutrophil surface markers tested compared to 14% of the WT iNeutrophils (Figure S3B). A list of surface proteins and expression percentages for WT iNeutrophils, *GATA1* KO iNeutrophils and primary neutrophils is available in Table S3.

The *GATA1* KO iNeutrophils produced a homogeneous forward- and side-scatter profile which largely localized to the previously determined neutrophil-like cell population seen in WT cells (Figures 1D, 1E, and 3D). The diffuse, non-neutrophil like population was dramatically reduced. Interestingly, the *GATA1* KO iNeutrophil population overlaps with the forward- and side-scatter profile seen in primary neutrophils (Figure 3D). Taken together, these results clearly show a remarkable similarity in surface protein expression, size, and granularity between the *GATA1* KO iNeutrophils and primary neutrophils.

GATA1 KO does not impact host defense functions

Neutrophils are a critical component of innate immunity and kill invading microorganisms through phagocytosis, MPO release, and ROS production. Analysis revealed that the *GATA1* KO iNeutrophils retained these important functions.

The WT and *GATA1* KO iNeutrophils were able to phagocytose human serum opsonized fluorescent microspheres *in vitro;* however, uptake in the WT cells was reduced relative to the *GATA1* KO cells (22%

vs. 41%). While the *GATA1* KO iNeutrophils had a slightly lower rate of phagocytosis relative to the primary neutrophils (46%), the GATA1 KO iNeutrophils were less variable. As expected, baseline phagocytosis was inhibited in all groups after treatment with the actin polymerization inhibitor cytochalasin D (Figures 4A and 4B).

The *GATA1* KO iNeutrophils retained their MPO activity to the same degree as WT iNeutrophils, but at elevated levels relative to primary neutrophils (Figure 4C). Additionally, WT and *GATA1* KO iNeutrophils along with primary neutrophils generated baseline ROS and were further stimulated through treatment with 10 nM phorbol myristate acetate (PMA). As expected, ROS production was inhibited with the selective protein kinase C (PKC) inhibitor sotrastaurin in all groups (Figure 4D).

GATA1 KO iNeutrophils form NETs like primary neutrophils

The formation of NETs was assessed in the WT and *GATA1* KO iNeutrophils after stimulation with PMA, the calcium ionophore A23187, and the bacterial toxin LPS. These stimulants were chosen because their mechanisms are well characterized, and they induce NETs using diverse pathways. Treatment with 50 nM PMA stimulated NETs in similar numbers of WT (50%) and *GATA1* KO iNeutrophils (51%), but less than primary neutrophils (66%) (Figure 5A). Similarly, A23187 was able to induce NETs in both WT and *GATA1* KO iNeutrophils, while WT iNeutrophils produced more NETs after stimulation (83%) compared to both *GATA1* KO iNeutrophils (62%) and primary neutrophils (51%) (Figure 5A). Considering both PMA and A23187 also generate extracellular traps (ETs) in other granulocytes, and flow cytometry determined that roughly 50% of the WT cells expressed the eosinophil surface marker Siglec-8, the large number of ETs seen in the WT iNeutrophils could be a product of non-neutrophil stimulation.

While LPS is a well-described, physiologically relevant NET stimulant, it failed to induce substantial NET formation in WT iNeutrophils (Figure 5A), highlighting a severe limitation with this cell model. Importantly, we observed that *GATA1* KO addresses this gap by fully restoring the ability to stimulate with LPS in iNeutrophils.

NET formation can be inhibited in _GATA1_ KO iNeutrophils as in primary neutrophils

PMA is a commonly used NET stimulant that activates PKC and subsequently generates ROS through the NADPH oxidase complex. This releases MPO and in turn helps decondense chromatin and expel DNA into the extracellular environment through the proposed pore-forming protein Gasdermin D. We investigated the pathway fidelity in both the WT and *GATA1* KO iNeutrophils using the PKC inhibitor sotrastaurin, the NADPH oxidase inhibitor diphenylene iodonium (DPI) and the MPO inhibitor 4-aminobenzoic acid hydrazide (4-ABAH). NET formation in the WT and *GATA1* KO iNeutrophils was substantially reduced after pre-treatment with these selective inhibitors. The reported Gasdermin D inhibitor disulfiram also dramatically reduced NETs in both WT and *GATA1* KO iNeutrophils, as expected (Figures 5B and 5C).

Alternatively, A23187 stimulates NET formation through peptidyl arginine deiminase 4 (PAD4) citrullination of histone H3 followed by chromosomal de-condensation, nuclear envelope rupture and DNA release through Gasdermin D. To test the fidelity of this pathway, we pre-treated the cells with the selective PAD4 inhibitor GSK484 before A23187 stimulation. As seen in primary neutrophils (31), inhibiting PAD4 almost completely rescued NET formation in the *GATA1* KO iNeutrophils (26% from 62%), but had a much less dramatic effect on WT KO iNeutrophils (66% from 83%). This demonstrates that stimulation with A23187 in the WT iNeutrophils is only partially PAD4 dependent, an observation seen in primary eosinophils (32). As expected, pre-treatment with disulfiram dramatically reduced NET formation in both the WT and *GATA1* KO iNeutrophils (Figures 5C and 5D).

GATA1 KO iNeutrophils can be genetically edited and used for target validation

CYBB encodes $p91^{phox}$, a component of the multi-protein NADPH oxidase complex that is important for PMA- and LPS-stimulated NET formation (31,33). To test whether *GATA1* KO iNeutrophils could be leveraged for functional genomic approaches, we knocked out *CYBB* using CRISPR/Cas9 in the *GATA1* KO hESCs, differentiated the cells to Day 19 iNeutrophils and stimulated the cells with PMA or LPS to induce NET formation. Upon stimulation with PMA, 44% of *GATA1* KO iNeutrophils with intact $p91^{phox}$ (control gRNA) generated NETs compared to 6% without $p91^{phox}$. Similarly, 72% of cells with WT $p91^{phox}$ generated NETs after LPS stimulation compared to 32% of cells without $p91^{phox}$ (Figures 6A and 6B).

These results establish that our *GATA1* KO iNeutrophils form NETs like primary neutrophils, and that NET formation can be inhibited pharmacologically and genetically. We conclude that *GATA1* KO iNeutrophils overcome a major limitation associated with primary neutrophils, by enabling the identification and validation of targets modulating neutrophil functions.

Discussion

In this study, we developed a novel method that dramatically increases the efficiency of differentiation, maturity, and functionality of hPSC-derived Neutrophils. Our method was adapted from previously published protocols to generate hematopoietic progenitors, with the addition of G-CSF between Day 12 and 18 to establish a granulocyte program, generating WT iNeutrophils. Recent reports optimizing the generation of iNeutrophils utilize gene overexpression to overcome differentiation challenges and deficiencies in host defense functions (37, 38). Overexpression and modification of genes can enhance iNeutrophil behavior *in vitro*, but strays from donor-derived neutrophils in ways that may not be readily apparent. These methods also require genetic manipulation during each round of cell production, adding delivery challenges and/or FACS to purify targeted cells. Unlike these protocols, our method is amenable to engineering at the self-renewing hPSC stage where modified cells can be expanded and banked for further use.

Flow cytometry analysis of WT iNeutrophils confirmed previous observations that they are composed of two distinct populations: one characterized by an immunophenotype typical of primary neutrophils, and

the other of either non-neutrophil granulocytes or hematopoietic progenitors. Sorting these two populations and comparing gene expression of five granulocyte-specific regulators revealed that the neutrophil-like population expressed low *GATA1* while the non-neutrophil population highly expressed *GATA1*.

From this observation, we hypothesized that knocking out *GATA1* in the hESCs before differentiation would push them towards neutrophils and away from other fates. hESCs with CRISPR/Cas9 deletion of *GATA1* expressed high levels of pluripotency genes, which were lost upon differentiation, consistent with the behavior and expression changes seen in WT cells. After hematopoietic induction, levels of the hematopoietic progenitor markers *SPI1* and *GFI1* rose in the Day 6 monolayer cells. Large numbers of cells began shedding off the supporting monolayer between Day 7 and Day 8, and floating *GATA1* KO cells on Day 12 expressed higher levels of neutrophil specific genes relative to the WT control, supporting our hypothesis that *GATA1* removal encourages a neutrophil program.

In line with these findings, flow cytometry analysis showed a very high degree of similarity between the *GATA1* KO iNeutrophils and primary neutrophils. Other methods report producing populations with roughly 50% CD11b positive cells, and low levels of CD66b (37). *GATA1* KO enhances neutrophil specification and produces greater than 95% CD11b+ and 85% CD66b+ cells, with 81% expressing all the neutrophil surface proteins tested, precluding time-consuming and resource-intensive sorting. Our method therefore constitutes a substantial improvement over previously described approaches.

Prior to this study, the formation of NETs in iNeutrophils has mostly been assessed using PMA, and while PMA does robustly activate specific NET pathways, it is not a physiologic stimulant. Additionally, PMA-stimulated ETs are not unique to neutrophils and occur in eosinophils (34,35). This suggests that PMA-stimulated ETs observed in cells made following previous iNeutrophil protocols (which generate heterogenous granulocyte populations) could be from non-neutrophil cells. Conversely, LPS is a physiologic bacterial cell wall component known to stimulate NETs *in vitro* in primary neutrophils, and by itself does not evoke DNA release in eosinophils (36). Furthermore, studies demonstrate differential production of ETs from neutrophils and eosinophils in human disease, stressing the mechanistic differences between the two cell types (37). Current iNeutrophil protocols generate heterogeneous populations of different granulocytes, and while these cells form PMA stimulated ETs, they likely do not capture the disease-relevant nuances of neutrophil-specific NETs. The relevance of these cells in NET studies is therefore limited.

The *GATA1* KO iNeutrophil model overcomes these limitations by generating pure cultures of neutrophil-like cells that respond to diverse NET stimulants like their primary counterpart. This is highlighted by the dramatic improvement in NET formation after stimulation with LPS, and the rescue of NET formation by A23187 after inhibition with GSK484 in the *GATA1* KO iNeutrophils.

While screens using primary neutrophils have uncovered drugs that inhibit NET formation (38), the targets of these drugs remain extremely challenging to pinpoint. Even if a ligand partner is discovered, this does not rule out off-target modalities. For instance, a group using the potent neutrophil elastase inhibitor GW311616A concluded neutrophil elastase is critical for NET formation (39). Follow up work employing selective neutrophil elastase inhibitors and knock-out mice dispute these findings, suggesting GW311616A's NET inhibition mechanism is likely off-target (40,41). Furthermore, validating targets using CRISPR/Cas9 knockouts in primary human cells is impossible due to the neutrophils' extremely short lifespan *ex vivo*, and the use of classic gene silencing techniques such as siRNA or shRNA may not be effective in neutrophils, which are rather stable and transcriptionally silent. Through the deletion of *CYBB*, we show how our iNeutrophils can provide a clean method to quickly validate targets without the uncertainty of compound off-target effects.

While targeting overactive NETs in disease is therapeutically attractive, interfering with other host-defense activities like phagocytosis and ROS release leave patients vulnerable to infections (42,43). Because *GATA1* KO iNeutrophils retain their other host defense capabilities, NET target knockout cells can serve as a tool to address the impact on these critical functions.

In conclusion, our differentiation method overcomes the limitations of previously published protocols by generating at-scale numbers of cells that are similar to primary neutrophils in form and function. COVID-19 highlights the link between dysregulated neutrophils and disease and stresses the therapeutic benefit of inhibiting unbalanced NETs. Our improved method accurately models NETs and enables large-scale screens and target validation in ways that were impossible using previous differentiation methods or primary neutrophils.

Acknowledgements: Matthias Mueller, Rob Maher, Haoyuan Liu, Eric Shikatani, Gianfranco de Pascale, Katie Worringer

Fig. 1. iNeutrophils generated using conventional differentiation methods are heterogeneous. (A) Schematic timeline of differentiation process including base media and soluble factor supplements. (B) Bright field images of differentiation at key timepoints. Scale bar = 100 µm. (C) Hematoxylin and eosin images of iNeutrophils harvested on Day 19 of differentiation compared to primary neutrophils. Scale bar = 20 µm. (D) Flow cytometry scatter plot of iNeutrophils collected on Day 19 of differentiation. Red gate surrounds high forward- and side-scatter population and blue gate surrounds low forward- and side-scatter population. (E) Flow cytometry analysis of blue and red gated populations from scatter plot. (F) Venn-diagram of neutrophil, eosinophil, and hematopoietic progenitor cell surface markers. (G) RT-qPCR

of *GFI1*, *CEBPD*, *GATA1*, *SPI1* and *CEBPB* performed on blue and red gated populations from (E) after sorting using FACS. Data normalized to GAPDH (n = 1 independent experiment; mean ± SD of technical triplicates).

Fig. 2. *GATA1 KO* improves iNeutrophil gene expression and phenotype. (A) RT-qPCR of pluripotency genes *OCT4*, *NANOG*, (B) hematopoietic transcription regulators genes *SPI1*, *GFI1*, (C) neutrophil specific genes *AZU1*, *AQP9*, *ELANE*, *MPO* (D) and the eosinophil and basophil gene *CLC* on Day 0, 6 and 12 of differentiation. Data is normalized to GAPDH and expressed as fold-change relative to WT hESCs (n = 3 independent experiments; mean ± SD). (E) Hematoxylin and eosin images of WT and *GATA1* KO iNeutrophils harvested on Day 19 of differentiation. Scale bar = 20 µm. (F) Number of floating cells produced by WT and *GATA1* KO cultures in each 6 cm dish on Day 19 (n = 4 independent experiments; mean ± SD). *P < 0.05 determined by unpaired t-test.

Fig. 3. *GATA1* KO iNeutrophils are immunophenotypically like primary neutrophils. (A) Schematic summary of proteins expressed on basophils, eosinophils and neutrophils. (B) Flow cytometry analysis of primary, WT and *GATA1* KO iNeutrophils stained using antibodies against non-neutrophil granulocyte surface markers CD49d, CD193 and Siglec-8 (C) and antibodies against neutrophil markers CD66b, CD182, CD15, CD16 and CD11b. Plots show isotype control (orange) and corresponding specific antibody (red) histograms. (D) Flow cytometry generated forward- and side-scatter plots of primary neutrophils, WT and *GATA1* KO iNeutrophils.

Fig. 4. *GATA1* KO iNeutrophils retain critical host defense functions. (A) Histograms represent phagocytosis of opsonized fluorescent microspheres in primary neutrophils, WT and *GATA1* KO iNeutrophils on Day 19 treated with DMSO (red) or 20 µM cytochalasin D (blue) along with (B) percentage uptake (n = 3 independent experiments; mean ± SD). (C) Myeloperoxidase (MPO) activity tested via chlorination in primary neutrophils, WT and *GATA1* KO iNeutrophils on Day 19 (n = 3 independent experiments; mean ± SD). (D) Reactive oxygen species (ROS) release in primary neutrophils, WT and GATA1 KO iNeutrophils on Day 19 after treatment with DMSO, 10 nM PMA or 10 nM PMA + 30 µM sotrastaurin. Values are presented as fold-change of mean fluorescent intensity relative to DMSO treated cells (n = at least 3 independent experiments; mean ± SD).

Fig. 5. *GATA1* KO iNeutrophils form NETs like primary neutrophils. (A) Percentage of primary neutrophils, WT and *GATA1* KO iNeutrophils undergoing NET formation after 3 hours of stimulation with DMSO, 25 µg/ml LPS, 50 nM PMA and 5 µg/ml A23187 on Day 19 (n = at least 3 independent

experiments; mean ± SD). (B) Fluorescent confocal microscopy of cells' nuclei (green) after stimulation with DMSO or 25 µg/ml LPS for 3 hours. Scale bar = 100 µm. (C) Percentage of primary neutrophils, WT and *GATA1* KO iNeutrophils undergoing NET formation after 1 hour pre-incubation with inhibitors followed by 3 hours of stimulation with 50 nM PMA or (D) 5 µg/ml A23187 on Day 19 (n = at least 3 independent experiments; mean ± SD). (E) Fluorescent confocal microscopy of cells' nuclei (green) after 1 hour pre-incubation with DMSO or 20 µM GSK484 followed by 3 hours of stimulation with 5 µg/ml A23187. Scale bar = 100 µm.

Fig. 5. NET target validation in *GATA1* KO iNeutrophils. (A) Percentage of non-targeting (control) and *CYBB* gRNA lentiviral transduced *GATA1* KO iNeutrophils undergoing NET formation after 3 hours of stimulation with DMSO, 25 µg/ml LPS or 50 nM PMA on Day 19 (n = at least 4 independent experiments; mean ± SD). (B) Fluorescent confocal microscopy of cells' nuclei (green) after stimulation with DMSO, 25 µg/ml LPS or 50 nM PMA for 3 hours. Scale bar = 100 µm.

References

1. Brinkmann V, Reichard U, Goosmann C, Fauler B, Uhlemann Y, Weiss DS, et al. Neutrophil Extracellular Traps Kill Bacteria. Science (1979). 2004 Mar 5;303(5663):1532–5.
2. Segal AW. How neutrophils kill microbes. Vol. 23, Annual Review of Immunology. 2005. p. 197–223.
3. Khandpur R, Carmona-Rivera C, Vivekanandan-Giri A, Gizinski A, Yalavarthi S, Knight JS, et al. NETs are a source of citrullinated autoantigens and stimulate inflammatory responses in rheumatoid arthritis. Sci Transl Med. 2013 Mar 27;5(178).
4. Qi H, Yang S, Zhang L. Neutrophil Extracellular Traps and endothelial dysfunction in atherosclerosis and thrombosis. Vol. 8, Frontiers in Immunology. Frontiers Media S.A.; 2017.
5. Hu SCS, Yu HS, Yen FL, Lin CL, Chen GS, Lan CCE. Neutrophil extracellular trap formation is increased in psoriasis and induces human β-defensin-2 production in epidermal keratinocytes. Sci Rep. 2016 Aug 5;6.
6. Grabcanovic-Musija F, Obermayer A, Stoiber W, Krautgartner WD, Steinbacher P, Winterberg N, et al. Neutrophil extracellular trap (NET) formation characterises stable and exacerbated COPD and correlates with airflow limitation. Respir Res. 2015 May 22;16(1).
7. Muñoz LE, Boeltz S, Bilyy R, Schauer C, Mahajan A, Widulin N, et al. Neutrophil Extracellular Traps Initiate Gallstone Formation. Immunity. 2019 Sep 17;51(3):443-450.e4.
8. Arcanjo A, Logullo J, Menezes CCB, de Souza Carvalho Giangiarulo TC, dos Reis MC, de Castro GMM, et al. The emerging role of neutrophil extracellular traps in severe acute respiratory syndrome coronavirus 2 (COVID-19). Sci Rep. 2020 Dec 1;10(1).
9. Veras FP, Pontelli MC, Silva CM, Toller-Kawahisa JE, de Lima M, Nascimento DC, et al. SARS-CoV-2-triggered neutrophil extracellular traps mediate COVID-19 pathology. Journal of Experimental Medicine. 2020 Dec 7;217(12).

10. Morris G, Bortolasci CC, Puri BK, Olive L, Marx W, O'Neil A, et al. Preventing the development of severe COVID-19 by modifying immunothrombosis. Vol. 264, Life Sciences. Elsevier Inc.; 2021.

11. Huang C, Wang Y, Li X, Ren L, Zhao J, Hu Y, et al. Clinical features of patients infected with 2019 novel coronavirus in Wuhan, China. The Lancet. 2020 Feb 15;395(10223):497–506.

12. Mokhtari T, Hassani F, Ghaffari N, Ebrahimi B, Yarahmadi A, Hassanzadeh G. COVID-19 and multiorgan failure: A narrative review on potential mechanisms. Vol. 51, Journal of Molecular Histology. Springer Science and Business Media B.V.; 2020. p. 613–28.

13. Laforge M, Elbim C, Frère C, Hémadi M, Massaad C, Nuss P, et al. Tissue damage from neutrophil-induced oxidative stress in COVID-19. Vol. 20, Nature Reviews Immunology. Nature Research; 2020. p. 515–6.

14. Zuo Y, Yalavarthi S, Shi H, Gockman K, Zuo M, Madison JA, et al. Neutrophil extracellular traps in COVID-19. JCI Insight. 2020 Jun 4;5(11).

15. Janiuk K, Jabłońska E, Garley M. Significance of nets formation in COVID-19. Vol. 10, Cells. MDPI; 2021. p. 1–12.

16. Adrover JM, Carrau L, Daßler-Plenker J, Bram Y, Chandar V, Houghton S, et al. Disulfiram inhibits neutrophil extracellular trap formation and protects rodents from acute lung injury and SARS-CoV-2 infection. JCI Insight. 2022 Mar 8;7(5).

17. Sinha S, Rosin NL, Arora R, Labit E, Jaffer A, Cao L, et al. Dexamethasone modulates immature neutrophils and interferon programming in severe COVID-19. Nat Med. 2022 Jan 1;28(1):201–11.

18. Blanter M, Gouwy M, Struyf S. Studying neutrophil function in vitro: Cell models and environmental factors. Vol. 14, Journal of Inflammation Research. Dove Medical Press Ltd; 2021. p. 141–62.

19. Kaufmann M, Schuffenhauer A, Fruh I, Klein J, Thiemeyer A, Rigo P, et al. High-throughput screening using iPSC-derived neuronal progenitors to identify compounds counteracting epigenetic gene silencing in fragile X syndrome. J Biomol Screen. 2015 Oct 22;20(9):1101–11.

20. Shinozawa T, Kimura M, Cai Y, Saiki N, Yoneyama Y, Ouchi R, et al. High-Fidelity Drug-Induced Liver Injury Screen Using Human Pluripotent Stem Cell-Derived Organoids. Gastroenterology. 2021 Feb 1;160(3):831–46.

21. Trump LR, Nayak RC, Singh AK, Emberesh S, Wellendorf AM, Lutzko CM, et al. Neutrophils Derived from Genetically Modified Human Induced Pluripotent Stem Cells Circulate and Phagocytose Bacteria In Vivo. Stem Cells Transl Med. 2019 Jun 1;8(6):557–67.

22. Brok-Volchanskaya VS, Bennin DA, Suknuntha K, Klemm LC, Huttenlocher A, Slukvin I. Effective and Rapid Generation of Functional Neutrophils from Induced Pluripotent Stem Cells Using ETV2-Modified mRNA. Stem Cell Reports. 2019 Dec 10;13(6):1099–110.

23. Lachmann N, Ackermann M, Frenzel E, Liebhaber S, Brennig S, Happle C, et al. Large-scale hematopoietic differentiation of human induced pluripotent stem cells provides granulocytes or macrophages for cell replacement therapies. Stem Cell Reports. 2015 Feb 10;4(2):282–96.

24. Chang Y, Syahirah R, Wang X, Jin G, Torregrosa-Allen S, Elzey BD, et al. Engineering chimeric antigen receptor neutrophils from human pluripotent stem cells for targeted cancer immunotherapy. Cell Rep. 2022 Jul 19;40(3).

25. Frenz S, Conca R, Hesse S, Linder MI, Klein C. Induced Pluripotent Stem Cell-Derived Neutrophil Granulocytes - Flow Cytometry Analysis Reveals Distinct Subpopulations. Blood. 2021 Nov 5;138(Supplement 1):3126–3126.

26. Hirasawa R, Shimizu R, Takahashi S, Osawa M, Takayanagi S, Kato Y, et al. Essential and instructive roles of GATA factors in eosinophil development. Journal of Experimental Medicine. 2002 Jun 3;195(11):1379–86.

27. Nei Y, Obata-Ninomiya K, Tsutsui H, Ishiwata K, Miyasaka M, Matsumoto K, et al. GATA-1 regulates the generation and function of basophils. Proc Natl Acad Sci U S A. 2013 Nov 12;110(46):18620–5.

28. Ditadi A, Sturgeon CM, Tober J, Awong G, Kennedy M, Yzaguirre AD, et al. Human definitive haemogenic endothelium and arterial vascular endothelium represent distinct lineages. Nat Cell Biol. 2015 May 5;17(5):580–91.

29. Heinze D, Park S, McCracken A, Haratianfar M, Lindstrom J, Villacorta-Martin C, et al. Notch activation during early mesoderm induction modulates emergence of the T/NK cell lineage from human iPSCs. Stem Cell Reports. 2022 Dec;17(12):2610–28.

30. Demetri GD, Griffin JD. Granulocyte colony-stimulating factor and its receptor. Blood. 1991 Dec 1;78(11):2791–808.

31. Kenny EF, Herzig A, Krüger R, Muth A, Mondal S, Thompson PR, et al. Diverse stimuli engage different neutrophil extracellular trap pathways. Elife. 2017 Jun 2;6.

32. Kim HJ, Sim MS, Lee DH, Kim C, Choi Y, Park HS, et al. Lysophosphatidylserine induces eosinophil extracellular trap formation and degranulation: Implications in severe asthma. Allergy: European Journal of Allergy and Clinical Immunology. 2020 Dec 1;75(12):3159–70.

33. Pieterse E, Rother N, Yanginlar C, Hilbrands LB, van der Vlag J. Neutrophils discriminate between lipopolysaccharides of different bacterial sources and selectively release neutrophil extracellular traps. Front Immunol. 2016 Nov 4;7(NOV).

34. Ueki S, Melo RCN, Ghiran I, Spencer LA, Dvorak AM, Weller PF. Eosinophil extracellular DNA trap cell death mediates lytic release of free secretion-competent eosinophil granules in humans. Blood. 2013 Mar 14;121(11):2074–83.

35. von Köckritz-Blickwede M, Goldmann O, Thulin P, Heinemann K, Norrby-Teglund A, Rohde M, et al. Phagocytosis-independent antimicrobial activity of mast cells by means of extracellular trap formation. Blood. 2008 Mar 15;111(6):3070–80.

36. Yousefi S, Gold JA, Andina N, Lee JJ, Kelly AM, Kozlowski E, et al. Catapult-like release of mitochondrial DNA by eosinophils contributes to antibacterial defense. Nat Med. 2008 Sep;14(9):949–53.

37. Hwang CS, Park SC, Cho HJ, Park DJ, Yoon JH, Kim CH. Eosinophil extracellular trap formation is closely associated with disease severity in chronic rhinosinusitis regardless of nasal polyp status. Sci Rep. 2019 Dec 1;9(1).

38. Sollberger G, Choidas A, Burn GL, Habenberger P, di Lucrezia R, Kordes S, et al. Gasdermin D plays a vital role in the generation of neutrophil extracellular traps. Sci Immunol. 2018 Aug 3;3(26):6689.

39. Papayannopoulos V, Metzler KD, Hakkim A, Zychlinsky A. Neutrophil elastase and myeloperoxidase regulate the formation of neutrophil extracellular traps. Journal of Cell Biology. 2010 Nov 1;191(3):677–91.

40. Kasperkiewicz P, Hempel A, Janiszewski T, Kołt S, Snipas SJ, Drag M, et al. NETosis occurs independently of neutrophil serine proteases. Journal of Biological Chemistry. 2020 Dec 18;295(51):17624–31.

41. Martinod K, Witsch T, Farley K, Gallant M, Remold-O'Donnell E, Wagner DD. Neutrophil elastase-deficient mice form neutrophil extracellular traps in an experimental model of deep vein thrombosis. Journal of Thrombosis and Haemostasis. 2016 Mar 1;14(3):551–8.

42. Danikas DD, Karakantza M, Theodorou GL, Sakellaropoulos GC, Gogos CA. Prognostic value of phagocytic activity of neutrophils and monocytes in sepsis. Correlation to CD64 and CD14 antigen expression. Clin Exp Immunol. 2008 Oct;154(1):87–97.

43. Quie PG, White JG, Holmes B, Good RA. In Vitro Bactericidal Capacity of Human Polymorphonuclear Leukocytes: Diminished Activity in Chronic Granulomatous Disease of Childhood. Journal of Clinical Investigation. 1967 Apr 1;46(4):668–79.

Figure 1

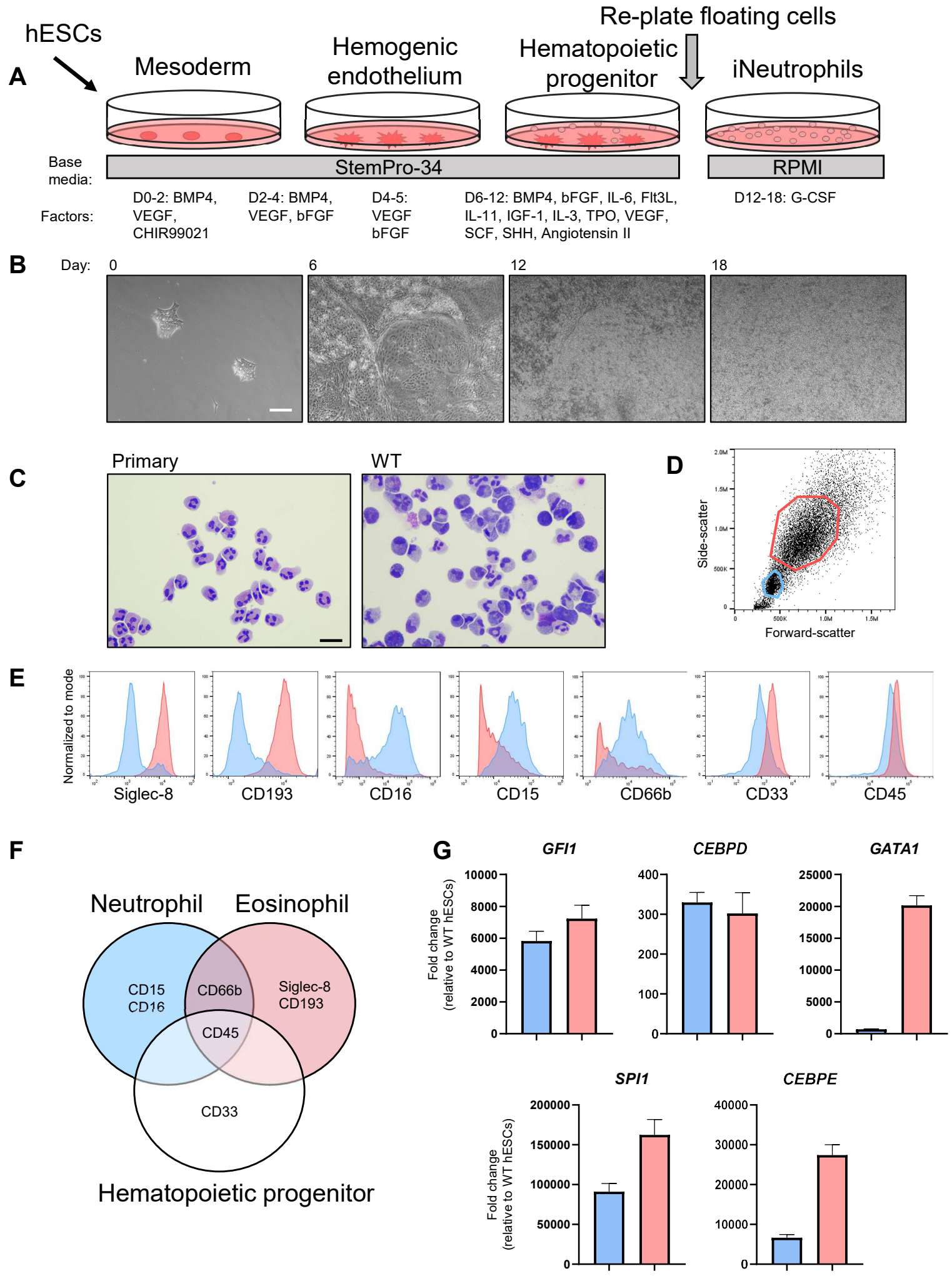
A
hESCs
Mesoderm
Hemogenic endothelium
Hematopoietic progenitor
Re-plate floating cells
iNeutrophils
Base media:
StemPro-34
RPMI
Factors:
D0-2: BMP4, VEGF, CHIR99021
D2-4: BMP4, VEGF, bFGF
D4-5: VEGF bFGF
D6-12: BMP4, bFGF, IL-6, Flt3L, IL-11, IGF-1, IL-3, TPO, VEGF, SCF, SHH, Angiotensin II
D12-18: G-CSF
B
Day: 0
6
12
18
C
Primary
WT
D
Side-scatter
Forward-scatter
E
Normalized to mode
Siglec-8
CD193
CD16
CD15
CD66b
CD33
CD45
F
Neutrophil
Eosinophil
CD15
CD16
CD66b
Siglec-8
CD193
CD45
CD33
Hematopoietic progenitor
G
GFI1
CEBPD
GATA1
SPI1
CEBPE
Fold change (relative to WT hESCs)

Figure 2

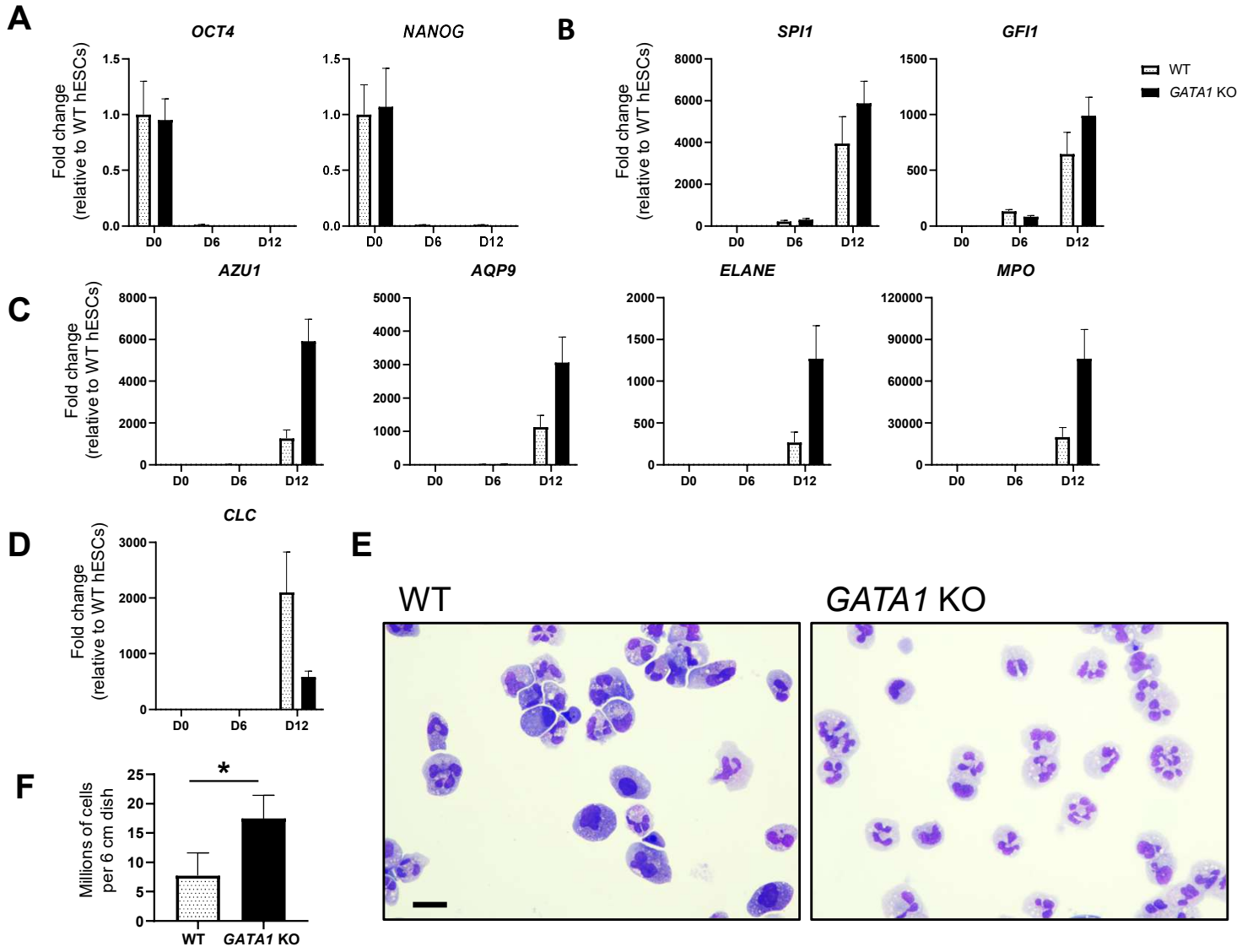
A
OCT4
NANOG
Fold change (relative to WT hESCs)
D0
D6
D12
B
SPI1
GFI1
WT
GATA1 KO
C
AZU1
AQP9
ELANE
MPO
D
CLC
E
WT
GATA1 KO
F
Millions of cells per 6 cm dish
*
WT
GATA1 KO

Figure 3

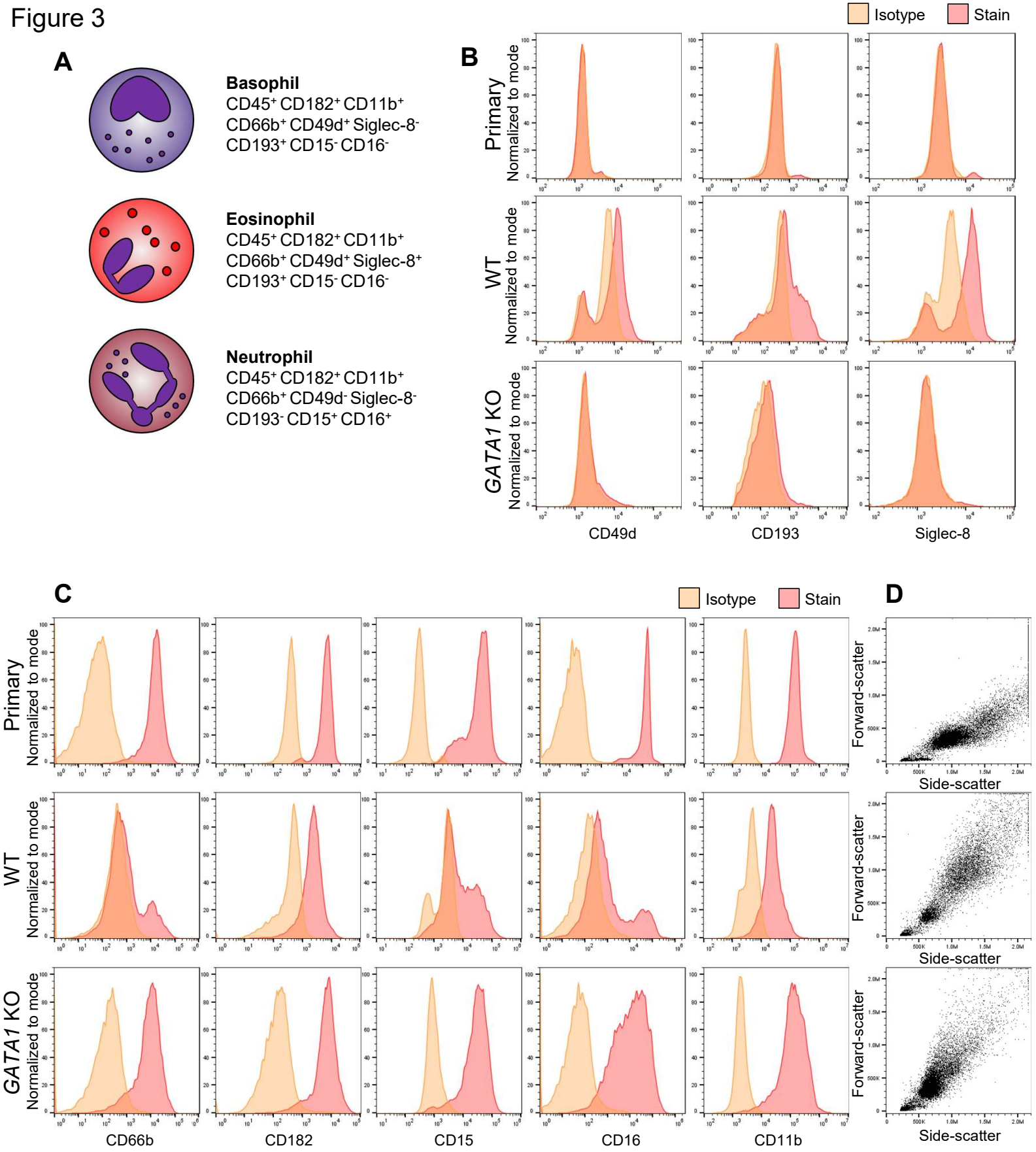
A
Basophil
CD45+ CD182+ CD11b+
CD66b+ CD49d+ Siglec-8-
CD193+ CD15- CD16-
Eosinophil
CD45+ CD182+ CD11b+
CD66b+ CD49d+ Siglec-8+
CD193+ CD15- CD16-
Neutrophil
CD45+ CD182+ CD11b+
CD66b+ CD49d- Siglec-8-
CD193- CD15+ CD16+
B
Isotype
Stain
Primary
WT
GATA1 KO
Normalized to mode
CD49d
CD193
Siglec-8
C
D
CD66b
CD182
CD15
CD16
CD11b
Forward-scatter
Side-scatter

Figure 4

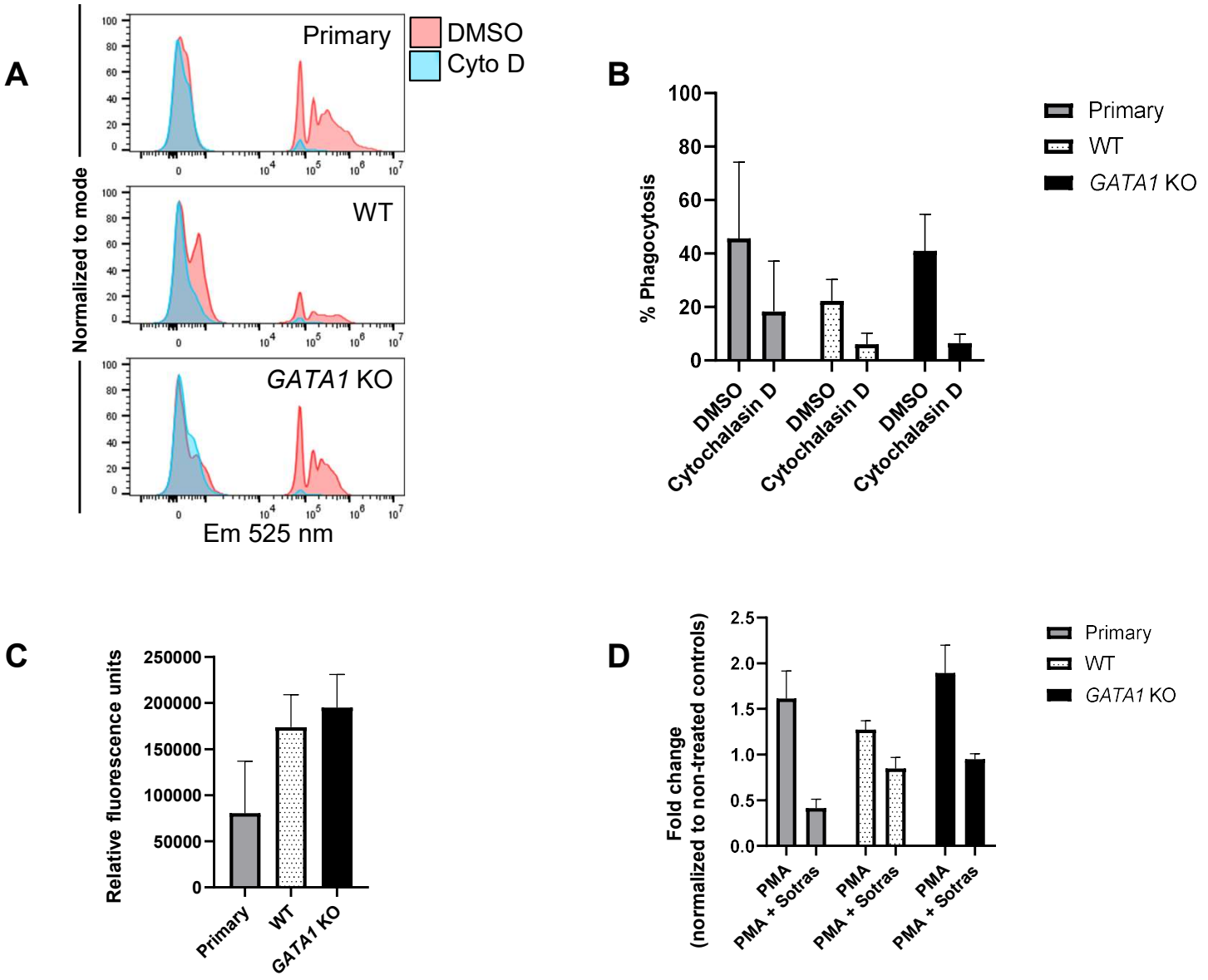
A
Primary
DMSO
Cyto D
WT
GATA1 KO
Normalized to mode
Em 525 nm
B
% Phagocytosis
Primary
WT
GATA1 KO
DMSO
Cytochalasin D
C
Relative fluorescence units
Primary
WT
GATA1 KO
D
Fold change
(normalized to non-treated controls)
Primary
WT
GATA1 KO
PMA
PMA + Sotras

Figure 5

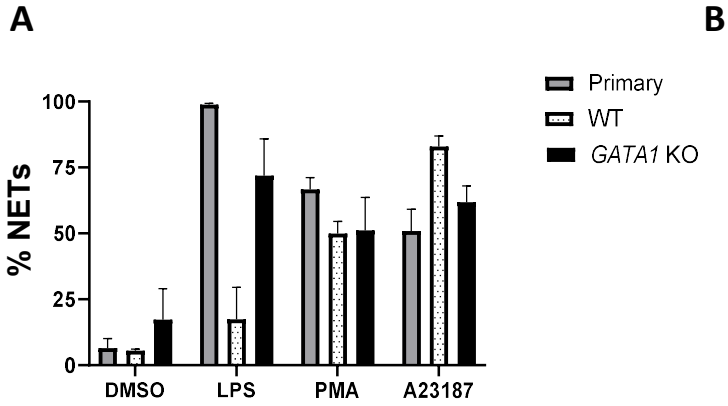
A
% NETs
100
75
50
25
0
DMSO
LPS
PMA
A23187
Primary
WT
GATA1 KO

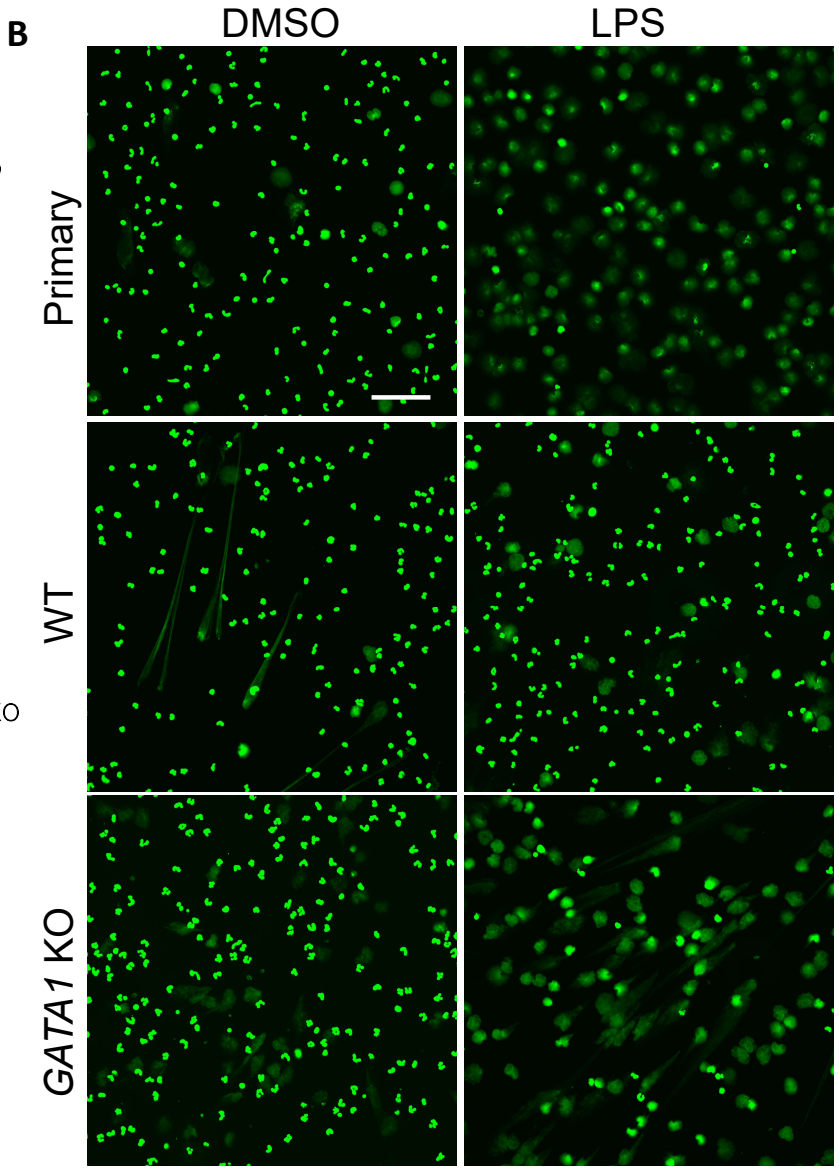
B
DMSO
LPS
Primary
WT
GATA1 KO

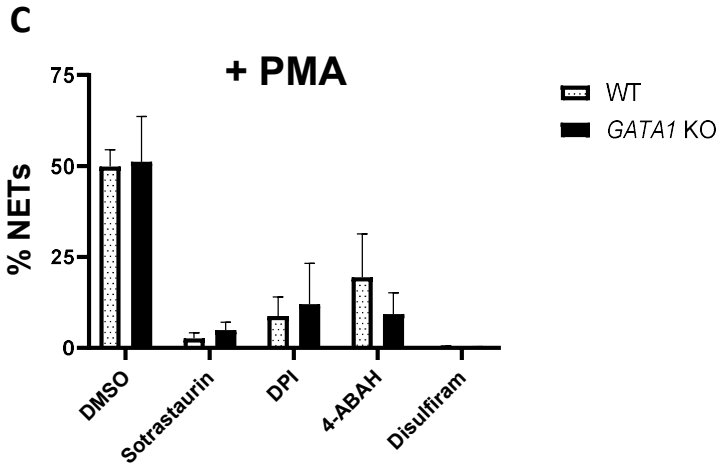
C
+ PMA
% NETs
75
50
25
0
DMSO
Sotrastaurin
DPI
4-ABAH
Disulfiram
WT
GATA1 KO

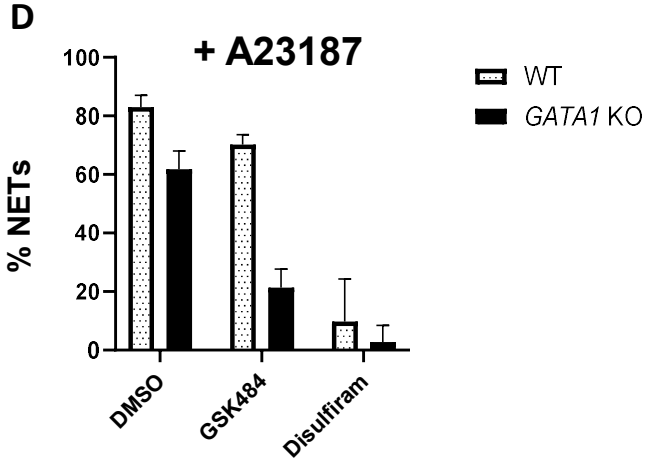
D
+ A23187
% NETs
100
80
60
40
20
0
DMSO
GSK484
Disulfiram
WT
GATA1 KO

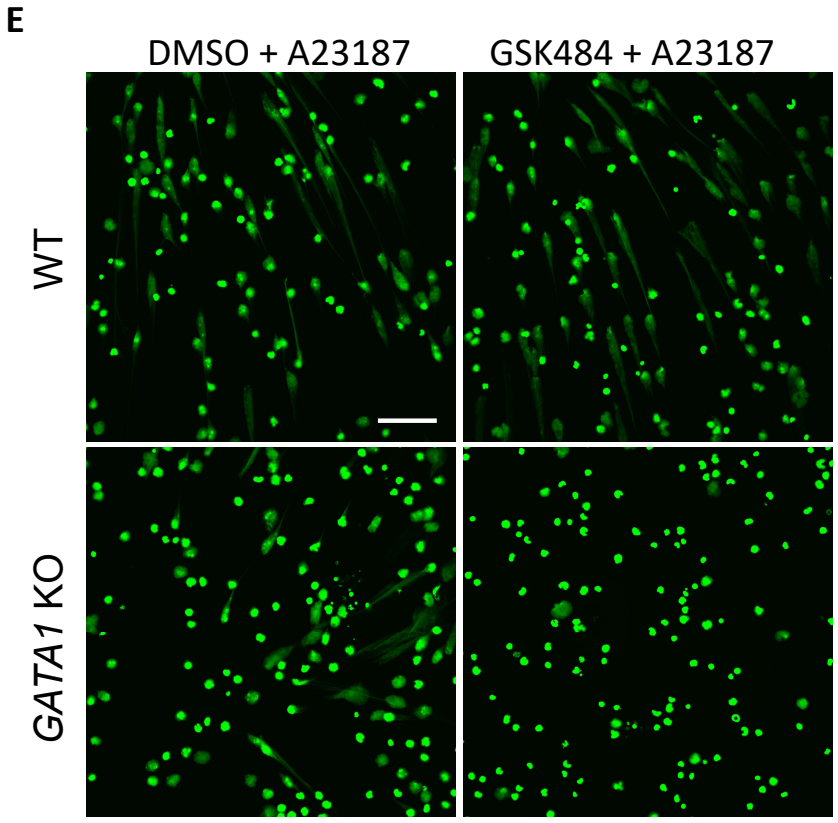
E
DMSO + A23187
GSK484 + A23187
WT
GATA1 KO

Figure 6

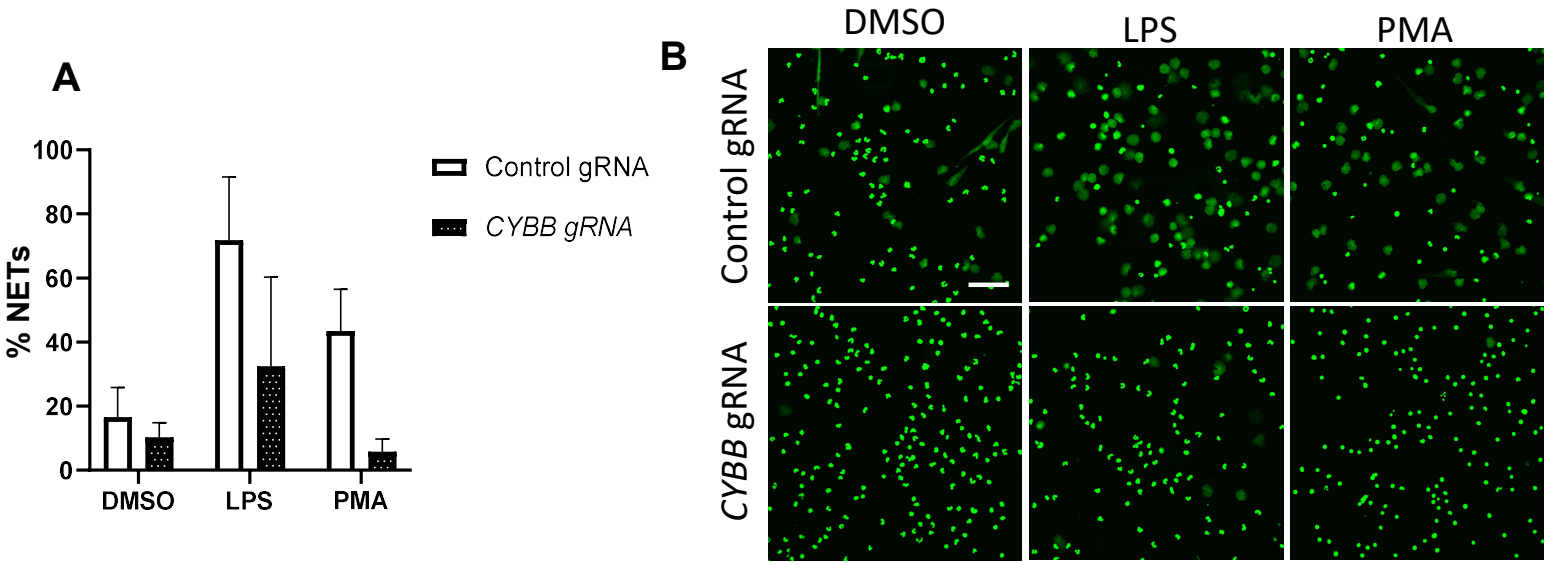
A
% NETs
100
80
60
40
20
0
DMSO
LPS
PMA
Control gRNA
CYBB gRNA
B
DMSO
LPS
PMA
Control gRNA
CYBB gRNA